RSC Advances

PAPER

View Article Online
View Journal | View Issue

Cite this: *RSC Adv.*, 2022, **12**, 26192

The origin of stability and high $Co^{2+/3+}$ redox utilization for $FePO_4$-coated $LiCo_{0.90}Ti_{0.05}PO_4$/MWCNT nanocomposites for 5 V class lithium ion batteries†

Naohisa Okita, [ab] Etsuro Iwama, [*abc] Yusuke Takami,[a] Shingo Abo,[a] Wako Naoi,[cd] Patrick Rozier,[bef] Patrice Simon, [bef] McMahon Thomas Homer Reid[bcg] and Katsuhiko Naoi [*abc]

Received 18th May 2022
Accepted 1st September 2022

DOI: 10.1039/d2ra03144b

rsc.li/rsc-advances

Highly-dispersed 10 wt% $FePO_4$ (FP)-coated $LiCo_{0.90}Ti_{0.05}PO_4$ (LCTP) was successfully synthesized within a multiwalled carbon nanotube matrix *via* our original ultracentrifugation process. 10 wt% FP-coated LCTP sample showed a higher discharge capacity of 116 mA h g^{-1} together with stable cycle performance over 99% of capacity retention at the 100th cycle in high voltage. A combination of TEM, XRD, XPS, and XAFS analyses suggests that (i) Ti^{4+}-substitution increases the utilization of Co redox (capacity increase) in LCP crystals by suppressing the Co_3O_4 formation and creating the vacancies in Co sites, and (ii) the FP-coating brought about the Fe enrichment of the surface of LCTP which prevents an irreversible crystal structure change and electrolyte decomposition during cycling, resulting in the stable cycle performance.

Introduction

In the ongoing quest to identify high-performance cathode materials for lithium-ion batteries (LIBs), one particularly promising candidate is $LiCoPO_4$ (LCP), in which P–O covalent bonding gives rise to a high redox potential of 4.8 V—significantly exceeding that of conventional materials such as $LiNi_{1/3}Co_{1/3}Mn_{1/3}O_2$ (4.5 V), $LiCoO_2$ (4.2 V), and $LiFePO_4$ (3.5 V).[1–3] Cathode materials with high reaction potential over 4.5 V are able to deliver a specific energy density that can reach 800 W h kg^{-1}.[4] Among cathode materials with high redox potential above 4.5 V, such as $Li(Ni_{1/2}Mn_{3/2})O_4$ (4.7 V) (ref. 5–7) and $LiNiPO_4$ (5.1 V),[8] LCP has excellent thermal and structural stability; $Li(Ni_{1/2}Mn_{3/2})O_4$ suffers capacity loss caused by manganese dissolution into electrolyte and poses a risk of ignition due to release of oxygen; $LiNiPO_4$ is plagued by a decrease in capacity due to the formation of intrinsic lattice defects as well as by the oxidation of electrolytes. LCP has a high theoretical capacity of 167 mA h g^{-1} compared to that of the conventional layered $LiCoO_2$ of 137 mA h g^{-1} with less Co weight fraction per formula unit. However, practical use of LCP is hampered by the poor rate-cycling capability of the material, which derives both from its inherently low electron conductivity[9] (<10^{-9} S cm^{-1}) and the poor Li^+ diffusivity[10] (<10^{-13} cm^2 s^{-1}) associated with the one-dimensional character of Li^+ diffusion along *b*-axis-oriented diffusion paths. A further impediment to practical use of LCP is the dramatic capacity degradation the material exhibits upon charge/discharge cycling, caused by electrolyte decomposition and structure deterioration. Although a number of mechanisms have been proposed to explain this phenomenon,[11–14] and although several studies using laboratory settings have used additives[11,15–18] or controlled voltage window[19] to yield improved cycle life up to 500 cycles. The low cyclability of LCP has so far hampered its use as a cathode material in LIBs. In our previous work,[20] we have shifted this paradigm by demonstrating that a combination of novel fabrication techniques and modified operating parameters can yield LCP-based materials, namely Fe-substituted LCP ($LiCo_{0.8}Fe_{0.2}PO_4$, LCFP), whose performance lies in an entirely different regime from that of previous studies and one much closer to what is required for practical applications. Indeed, our LCFP cells exhibited cycle life in excess of 5000 cycles with >85% capacity retention despite requiring no additives of any kind. This improvement was the product of

[a]*Department of Applied Chemistry, Tokyo University of Agriculture & Technology, 2-24-16 Naka-cho, Koganei, Tokyo 184-8588, Japan. E-mail: n-okita@go.tuat.ac.jp; iwama@cc.tuat.ac.jp; k-naoi@cc.tuat.ac.jp*

[b]*Global Innovation Research Organization, Tokyo University of Agriculture & Technology, 2-24-16 Naka-cho, Koganei, Tokyo, 184-8588 Japan*

[c]*Advanced Capacitor Research Center, Tokyo University of Agriculture & Technology, 2-24-16 Naka-cho, Koganei, Tokyo 184-8588, Japan*

[d]*Division of Art and Innovative Technologies, K & W Inc., 1-3-16-901 Higashi, Kunitachi, Tokyo 186-0002, Japan*

[e]*Réseau sur le Stockage Electrochimique de l'Energie (RS2E), France CNRS 3459*

[f]*CIRIMAT, Université de Toulouse, CNRS, Université Toulouse 3 – Paul Sabatier, 118 Route de Narbonne, 31062 Toulouse Cedex 9, France*

[g]*Simpetus LLC., 1 Fitchburg St, Somerville, MA 02143, USA*

† Electronic supplementary information (ESI) available. See https://doi.org/10.1039/d2ra03144b

multiple factors: (i) the formation of an Fe-rich surface layer—assisted by the fabrication step of ultracentrifugation (UC)—that served to stabilize the crystal against lattice expansion during high-voltage operation, (ii) the creation of vacancies at Co sites in the crystal structure that enhance the Li^+ diffusivity in LCFP crystals and decrease its charge transfer resistance and (iii) the restriction of the operating voltage range to ensure that Fe remains oxidized at valence state 3+. Although each of these factors was clearly identified in our previous work, the interrelations among them were left unexplored, as were optimal recipes for material fabrication and device configuration.

In this paper, we extend our work in several ways, clarifying the mechanisms responsible for the improved performance of our LCFP and exploiting this understanding to optimize material design and fabrication, ultimately yielding cells with improved performances. A key breakthrough enabling this progress is an improved understanding of the distinct mechanisms governing the relevant surface and bulk phenomena and of their mutual interactions. The main novelties of this study is the challenge to design the stable and high voltage $LiCo_{0.90}Ti_{0.05}PO_4$ (LCTP) cathode material with $FePO_4$(FP)-coating by separately controlling the outer ($FePO_4$-coating)[21] and inner (Ti^{4+}-substitution of Co^{2+}) parts of LCP nanoparticles. The former with annealing process under air leads to the formation of Fe-rich surface layer, which suppresses the degradation reaction such as Li/Co cation mixing and electrolyte oxidative decomposition and drastically improves cyclability of LCP cathode materials. The latter leads to the creation of vacancies which effectively increases the capacity of LCP cathode with an increment of utilization of $Co^{2+/3+}$ redox reaction. Our previous work reported Fe^{3+}-substituted LCP, *i.e.*, LCFP, which successfully improves cyclability of LCP cathode material. However, the synthesis of such $LiCo_{0.8}Fe_{0.2}PO_4$ failed to control the behavior of surface and inner core of LCP nanoparticles, and thus sacrificed the capacity of LCP with the cyclability improvement. We believe that this work offers new strategies to improve different electrochemical properties of LCP as well as other high voltage cathode materials *via* separate control of surface/bulk properties of nanoparticles. As replacements for the Fe dopants, we consider doping with different elements and use X-ray and neutron-diffraction analysis to study the effect of dopant concentration on the formation of vacancies in the crystal structure. We find that among various tested elements Ti^{4+} is the most effective dopant, and we suggest possible explanations for this finding. Finally, this work results in significant of capacity improvement of the FP-coated LCTP material (116 mA h g-active material^{-1}, 87 mA h g-composite^{-1}) compared to that of raw LCFP (95 mA h g-active material^{-1}, 67 mA h g-composite^{-1})[20] as well as outstanding cycling stability. Our findings offer new strategies for improving cycle performance without sacrificing the capacity of LCP, paving the way toward the realization of high voltage LIBs.

Results and discussion

In previous recent works,[20–24] we showed that the design of an $FePO_4$-coating onto $LiCoPO_4$ (FP-coated LCP) particles resulted in improved cyclability ascribed to the formation of a protective Fe^{3+}-rich surface layer onto LCP. The FP-coating also brought about an improvement of Li diffusivity ascribed to partial migration of Fe^{3+} in the LCP structure accompanying with a formation of vacancies in M2 (Co^{2+}) sites for charge compensation. To further enhance the electrochemical properties of bulk LCP, we selected Ti^{4+} to prepare aliovalent-substituted LCP ($LiCo_{1-2x}Ti_xPO_4$) expecting that the 4+ valence state will allow the creation of more vacancies[25–27] in the bulk LCP crystal than using Fe^{3+}. Among the various tested samples with different dopant concentrations, the highest discharge capacity of 102 mA h g^{-1} (normalized to LCTP weight) and 71 mA h g^{-1} (composite weight, the carbon content were calculated by thermogravimetric/differential thermal analyzer (TG/DTA) as shown Fig. S1†) at the initial cycle was obtained for $x = 5$ at% of Ti doping (see Fig. S2 and S3†). We also found that LCTP surpassed LCFP and LCP in terms of discharge capacity. As shown in Fig. 1a–c and 1e, the capacity retention of such $LiCo_{0.90}Ti_{0.05}PO_4$ (LCTP) was 72% after 100 cycles. This value is better than uncoated LCP but fails to be as good as Fe-substituted sample. Having identified LCTP as a material offering high capacity but limited cycle performance, we attempted to improve its cyclability by FP-coating. As shown in Fig. 1d and e, FP-coating leads to a drastic improvement of the capacity retention since no capacity decrease was observed over 100 cycles and even better capacity than un-coated LCTP (116 mA h g^{-1} normalized to FP-coated LCTP weight and 87 mA h g^{-1} composite weight). We also performed the 1C-rate cyclability tests for the FP-coated LCTP/MWCNT up to 500th cycles with a 83% capacity retention as shown in Fig. 1f. Comparison of charge/discharge curves for LCP and LCTP with and without FP coating suggests that the surface protection of LCP/LCTP particles plays an important role in the stabilization. To go further in the understanding of the specific role of Ti^{4+} and FP-coating on the electrochemical performances of LCP, we achieved a deep analysis of the materials.

X-ray diffraction (XRD) patterns of all three samples (uncoated LCP, uncoated LCTP, and FP-coated LCTP) were recorded and are reported in Fig. 2. All main diffraction peaks can be indexed using an olivine-type structure (S.G. *Pnma* $LiCoPO_4$: JCPDS card no. 85-0002). Apart low-intensity peaks assigned to multiwalled carbon nanotubes and Co_3O_4, no other peaks were detected, indicating successful synthesis of crystalline $LiCoPO_4$ as well as all other LCP derivatives synthesized in this study. The evaluated ratios of Co_3O_4 in the different samples (Table 1) show that the Ti-doping and FP-coating are both effective to suppress the formation of Co_3O_4 phase. Electrochemical performances of samples with different Ti content show that 5% of Ti lead to optimal properties (see Fig. S2†) and thus it was concluded that the 5% was the upper limit of Ti concentration for the LCTP solid solution. Positions of some Bragg peaks being shifted by 5% Ti-substitution or FP-coating (see Fig. S4†). Lattice parameters for the three samples were refined from both XRD patterns (Table 1a) and neutron powder diffraction patterns (NPD) (Table 1b). The refined lattice parameters are consistent between two diffraction data and show that the 0.05 Ti-substitution in LCP induces little changes

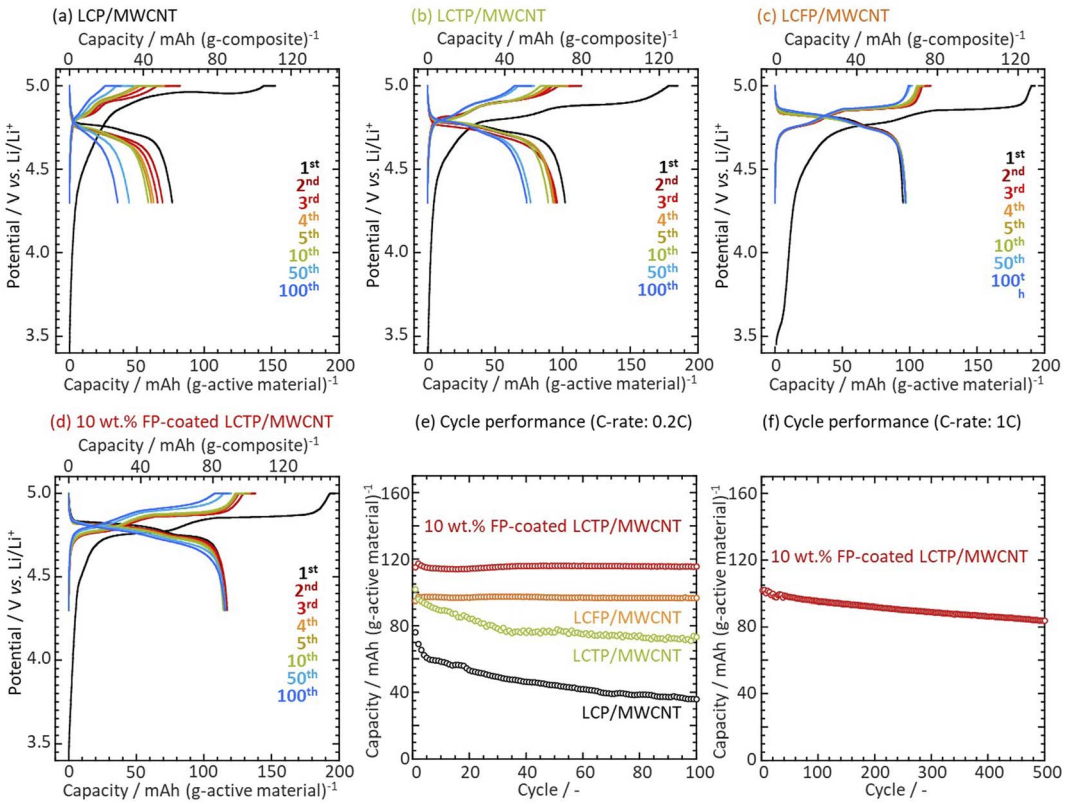

Fig. 1 Charge discharge curves of (a) LCP, (b) LCTP, (c) LCFP and (d) FP-coated LCTP/MWCNT cathodes in 1 M $LiPF_6$ in EC : PC : DMC (1 : 1 : 3 in vol.) operated at CC–CV charge (0.2C-rate) and CC discharge (0.2C-rate). Confined operation voltage: 4.3–5.0 V *vs.* Li was applied as reported in our previous works.[20,21] Capacity plots against cycle number for a Li metal half-cell using composites at (e) a 0.2C-rate and (f) a 1C-rate.

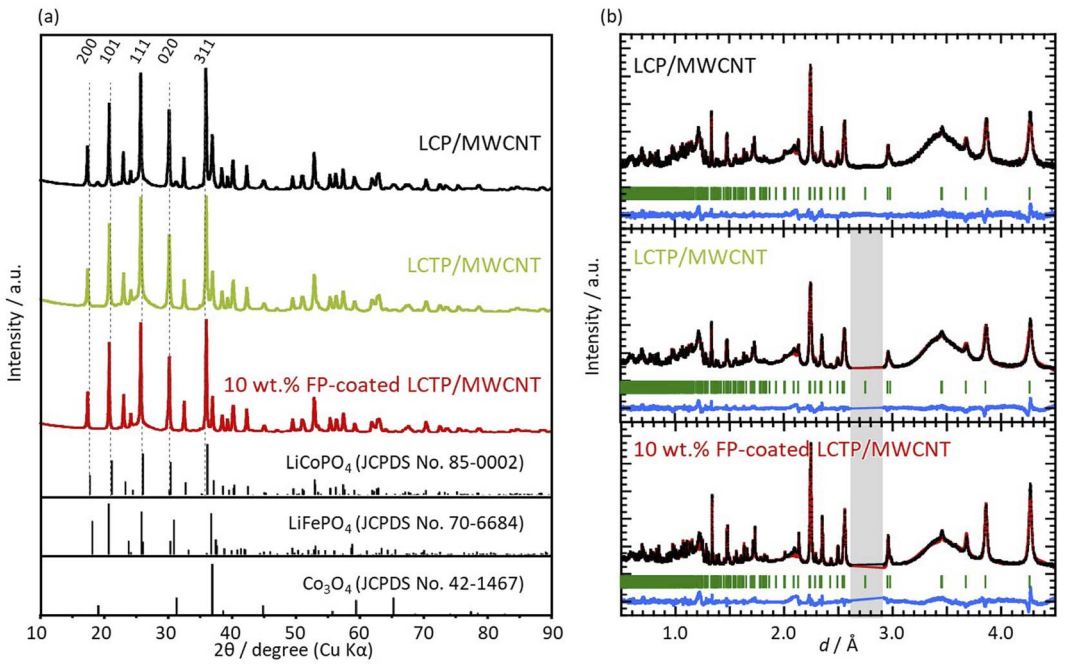

Fig. 2 (a) X-ray diffraction patterns for the three composites: LCP, LCTP, and FP-coated LCTP/MWCNT composites. (b) Neutron diffraction patterns for LCP, LCTP, and FP-coated LCTP/MWCNT composites. Grey area corresponds to the noise related to synchrotron measurements, which was not taken into account for any fitting.

Table 1 Lattice parameters refined using (a) X-ray and (b) neutron diffraction patterns for the three composites: LCP, LCTP, and FP-coated LCTP/MWCNT. (c) The results of Rietveld refinement of neutron diffraction patterns for the three composites

(a) Lattice parameters calculated by XRD patterns

Sample	Space group	a/Å	b/Å	c/Å	V/Å^3	R_{wp}	R_p	R_e	S	χ^2	Co_3O_4 ratio calculated by XRD/wt%
$LiCoPO_4$	*Pnma*	10.2023(7)	5.9219(4)	4.7001(3)	283.97(3)	5.89	4.36	3.21	1.83	3.36	9.9
$LiCo_{0.9}Ti_{0.05}PO_4$	*Pnma*	10.1972(8)	5.9229(4)	4.7025(4)	284.02(4)	4.09	3.00	2.90	1.41	1.98	0.6
10 wt% $FePO_4$-coated $LiCo_{0.9}Ti_{0.05}PO_4$	*Pnma*	10.1877(4)	5.9192(3)	4.7036(2)	283.64(2)	4.73	3.43	2.89	1.64	2.68	0

(b) Lattice parameters calculated by NPD patterns

Sample	Space group	a/Å	b/Å	c/Å	V/Å^3	R_{wp}	R_p	R_e	S	χ^2
$LiCoPO_4$	*Pnma*	10.202(1)	5.9233(7)	4.7006(4)	284.05(5)	4.54	3.44	1.91	2.37	5.63
$LiCo_{0.9}Ti_{0.05}PO_4$	*Pnma*	10.192(1)	5.9220(6)	4.7021(3)	283.81(4)	4.97	3.66	1.39	3.58	12.82
10 wt% $FePO_4$-coated $LiCo_{0.9}Ti_{0.05}PO_4$	*Pnma*	10.1864(4)	5.9193(2)	4.7035(2)	283.61(2)	7.83	5.64	1.59	4.93	24.27

(c) Rietveld refinement results of NPD patterns

		Wyckoff	x/a	y/b	z/c	B_{Iso}	Occupancy
$LiCoPO_4$							
M1 site (Li site)	Li^+	4a	0	0	0	3.8(2)	1.00(2)
M2 site (Co site)	Co^{2+}	4c	0.2749(3)	0.25	1.0048(9)	1.77(9)	1.00(1)
	P	4c	0.0906(2)	0.25	0.4190(3)	0.64(3)	1
	O^-	4c	0.0991(1)	0.25	0.7480(3)	0.52(3)	1
	O^-	4c	0.4537(1)	0.25	0.2076(3)	0.92(3)	1
	O^-	8d	0.1667(1)	0.0485(1)	0.2837(2)	1.02(2)	1
$R_{wp} = 4.54$, $R_p = 3.44$, $R_e = 1.91$, $S = 2.37$, $\chi^2 = 5.63$							
$LiCo_{0.9}Ti_{0.05}PO_4$							
M1 site (Li site)	Li^+	4a	0	0	0	4.0(1)	1.000(2)
M2 site (Co site)	Co^{2+}	4c	0.2712(3)	0.25	1.0016(7)	1.58(7)	0.900(4)
	Ti^{4+}	4c	0.2712(3)	0.25	1.0016(7)	1.58(7)	0.050(1)
	P	4c	0.0902(1)	0.25	0.4212(2)	0.86(2)	1
	O^-	4c	0.09987(9)	0.25	0.7497(2)	0.73(2)	1
	O^-	4c	0.45428(8)	0.25	0.2040(2)	1.11(2)	1
	O^-	8d	0.16691(7)	0.0474(1)	0.2804(2)	1.34(2)	1
$R_{wp} = 4.97$, $R_p = 3.66$, $R_e = 1.39$, $S = 3.58$, $\chi^2 = 12.8$							
10 wt% $FePO_4$-coated $LiCo_{0.9}Ti_{0.05}PO_4$							
M1 site (Li site)	Li^+	4a	0	0	0	3.23(8)	1.000(3)
M2 site (Co site)	Co^{2+}	4c	0.2761(1)	0.25	0.9922(3)	1.90(4)	0.794(1)
	Ti^{4+}	4c	0.2761(1)	0.25	0.9922(3)	1.90(4)	0.0981(5)
	Fe^{3+}	4c	0.2761(1)	0.25	0.9922(3)	1.90(4)	0.0273(6)
	P	4c	0.2761(1)	0.25	0.4182(1)	0.86(1)	1
	O^-	4c	0.10012(5)	0.25	0.7469(1)	0.79(1)	1
	O^-	4c	0.45298(5)	0.25	0.2022(1)	0.86(1)	1
	O^-	8d	0.16708(4)	0.04686(6)	0.2813(9)	1.13(1)	1
$R_{wp} = 7.83$, $R_p = 5.64$, $R_e = 1.59$, $S = 4.93$, $\chi^2 = 24.3$							

in the lattice parameters. In contrast to uncoated LCP and LCTP, an evolution of lattice parameters for FP-coated sample is observed with decreasing of the a and b parameters and increasing of the c one. This indicates that Fe ions partially dissolves into the LCTP bulk crystal structure coinciding with the FP coating on the nanoparticle surface. Such assumption of the Fe ions presence in the M2 sites was supported by the combination of X-ray photoelectron spectroscopy (XPS) (Fig. 3) and NPD analysis. From the XPS depth profiles shown in Fig. S5† in the original manuscript, the Fe ratio in the total ratio of transition metals (Fe + Co + Ti) after 30 s Ar etching remained 28%, suggesting that the dissolution of Fe ions within the inner part of LCTP nanoparticles. The NPD analysis confirmed the substitution of Co^{2+} at M2 site with Fe^{3+} (Table 1c), as the sum of refined site occupancies in M2 sites failed to reach 1.00 for two LCTP samples. The fact that the vacancies lie in M2 (Co^{2+}) sites is consistent with previous reports.[20,22,25–29] The highest amount of vacancies is obtained for the FP-coated LCTP which combines both effect of Ti^{4+} and Fe^{3+}-substitution for Co^{2+}, leading to the highest exhibited capacity as observed in Fig. 1.

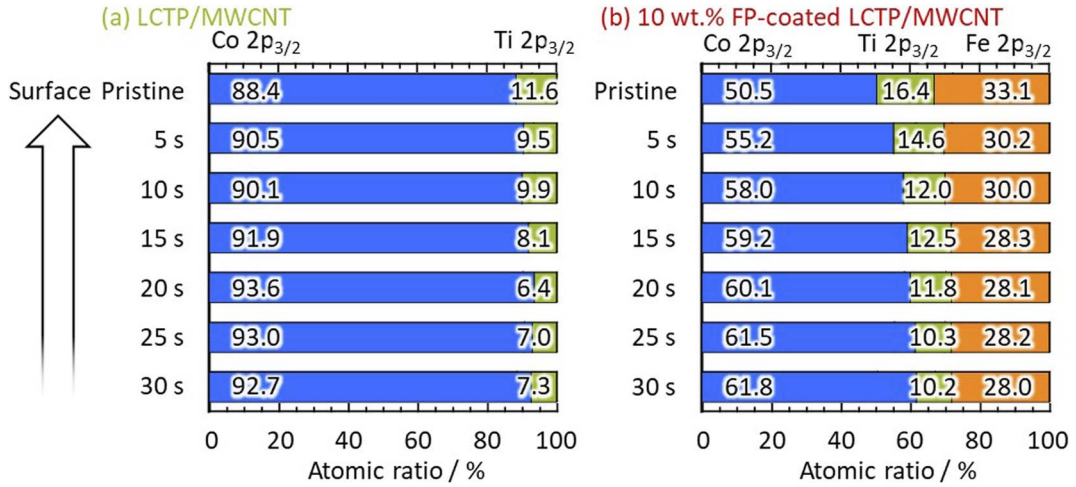

Fig. 3 Consecutive XPS measurements with data acquisition at 5 s intervals during 0–30 s Ar ion etching. Atomic ratio of Co, Ti, and Fe calculated from depth profiles (see Fig. S5†) for (a) LCTP and (b) FP-coated LCTP/MWCNT composites.

However, for a higher content of Ti (10%), the capacity decreases due to the formation of side products, such as $LiTi_2(PO_4)_3$ (see Fig. S2†). XPS analyses of Co $2p_{3/2}$, Ti $2p_{3/2}$, and Fe $2p_{3/2}$ were performed on the LCTP particles with or without FP coating, using Ar ion etching to track the change of the composition from the surface into the bulk of the particles (Fig. S5 and S6†). Fig. 3 shows the Co/Ti, Co/Fe, and Co/Ti/Fe ratios calculated by integrating the areas under the Co $2p_{3/2}$, Ti $2p_{3/2}$, and Fe $2p_{3/2}$ peaks. Examination of the results for LCTP particles shows that the distribution of Co and Ti at the surface (Co/Ti = 88/12) only slightly differs from that in the bulk (Co/Ti = 93/7). Differently, the FP-coating drastically changed the surface composition, suggesting the successful formation of an Fe^{3+}-rich phase on the LCTP crystals, as we previously reported for LCFP and FP-coated LCP.[20,21]

To determine the effect of Ti-substitution and FP-coating on the redox state of Co and Fe, *in situ* X-ray adsorption fine structure (XAFS) measurements were conducted for the three different samples at 1st and 50th cycle. The X-ray absorption near edge structure (XANES) spectra of Co, Fe and Ti K-edge for the LCP and LCTP composites with or without FP-coating are shown in Fig. S7.† Beside the analysis showing that Ti remains in +4 valence state, the valence states of Co and Fe in the composite are determined by deconvolving the spectra using the contributions of Co^{2+}, Co^{3+}, Fe^{2+} and Fe^{3+}. As shown in Table 2, different Co valence states are determined for the three as-prepared electrodes, where those in LCTP samples corresponds to Co = +2 regardless of FP-coating, while LCP sample show Co = +2.13. The difference of Co valence states between uncoated LCP and LCTP, which equals to 0.13, cannot be simply explained by the different amounts of Co_3O_4 (average valence state Co = +2.66) impurity crystalline phase evaluated from the XRD patterns fitting (10%, see Table 2). Such difference may be related to the accuracy of the method or the presence of amorphous Co oxides. Although the explanation of such difference is still unspecified, the role of Ti^{4+} and generated vacancies can be suggested to favor the stabilization of Co in electrochemically active +2 valence state leading to increased capacity compared to undoped LCP sample which contains some electrochemically inactive Co_3O_4. During the first cycle, at the charged state, the Co valence state increases, and reaches much higher value for FP-coated sample (+2.82) compared to uncoated one (+2.66), which is well consistent with the increased capacity measured and with the obtained galvanostatic intermittent titration technique plots (Fig. S8†). The comparison of the Co valence state at charged state along cycles shows that after 50 cycles the numbers for the FP-coated LCTP remained almost same while those for uncoated ones clearly decreased, being in good agreement with already discussed capacity retention capabilities. *Ex situ* XRD analysis (Fig. S9†) supports such stability of FP-coated samples indicating that the unit cell volume for coated samples remains constant after 50 cycles, while the one for uncoated samples increases (Table S1†). This increase can be explained in light of reported data by the existence of a progressive cation mixing in uncoated LCP or LCTP crystals, accompanied by the decay of crystal structure. This explanation is supported by the HRTEM images of the sample after cycling (Fig. 4). HRTEM images observed on three composites indicated that all composites contain nanocrystals of *ca.* 100 nm highly dispersed within the MWCNT matrix (Fig. 4a–c). Magnified images for the LCP/MWCNT and LCTP/MWCNT composites showed a highly crystalline bulk part of LCP or LCTP surrounded by amorphous phase (Fig. 4d–f). The crystalline bulk part of LCP and LCTP showed clear lattice fringes with interplanar lattice distances of 4.3 and 3.5 Å corresponding to the (101) and (111) planes of the olivine structure, respectively. The interplanar lattice distance of FP-coated LCTP observed in Fig. 4f is 5.1 Å, which well agreed with the (200) plane of the olivine structure, indicating the successful FP-coating and partial dissolution of Fe^{3+} into the LCTP crystalline. After 50 cycles, the lattice fringes for the LCP and LCTP without FP-coating disappeared, indicating the crystal structural decay (Fig. 4g and h). In the other hand, the lattice fringes

Table 2 Formal valence number of Co and Fe evaluated from XAFS spectra for the half-cells consisting of Li/1 M $LiPF_6$ EC : PC : DMC(1 : 1 : 3 in vol.)/(LCTP/MWCNT composite) at 1st and 50th cycles

		Co valence state			Fe valence state		Equivalent Co_3O_4 ratio calculated by XAFS[a]/wt%
Sample	Cycle no.	OCV/discharge State	Charge state	Change in Co valence state	OCV/discharge State	Charge state	
LCP/MWCNT	1st	+2.13	+2.66	0.53	—	—	19.7
	50th	+2.13	+2.47	0.34	—	—	—
LCTP/MWCNT	1st	+2.00	+2.67	0.66	—	—	0
	50th	+2.03	+2.57	0.54	—	—	—
10 wt% FP-coated LCTP/MWCNT	1st	+2.00	+2.82	0.82	+2.74	+3.06	0
	50th	+2.00	+2.81	0.81	+2.93	+2.98	—

[a] This ratio is equivalent for Co_3O_4 calculated by valence number of Co.

for the FP-coated LCTP samples remained clearly visible, which well agrees with its excellent cyclability (Fig. 4i).

As initially shown in this manuscript, the Ti^{4+}-substitution increased the capacity and the utilization of Co^{2+}/Co^{3+} in LCP, but did not improve its cycling performance (Fig. 1e). Upon cycling, LCTP suffers both structural degradation (Li–Co cation mixing) and SEI accumulation on the particle surface due to the electrolyte decomposition, as evidenced by in XRD patterns (Fig. S9†) and TEM images (Fig. 4). It was the FP-coating to LCTP/MWCNT which improved the cycling performance of LCTP/MWCNT. The FP-coating brought about both the formation of Fe^{3+}-rich surface on LCP particles, resulted in the suppression of electrolyte decomposition and subsequent cation mixing. Combining the XAFS analysis with XPS and TEM, the surface Fe^{3+} enrichment brings about the stability enhancement of the delithiated phase, leading to excellent long

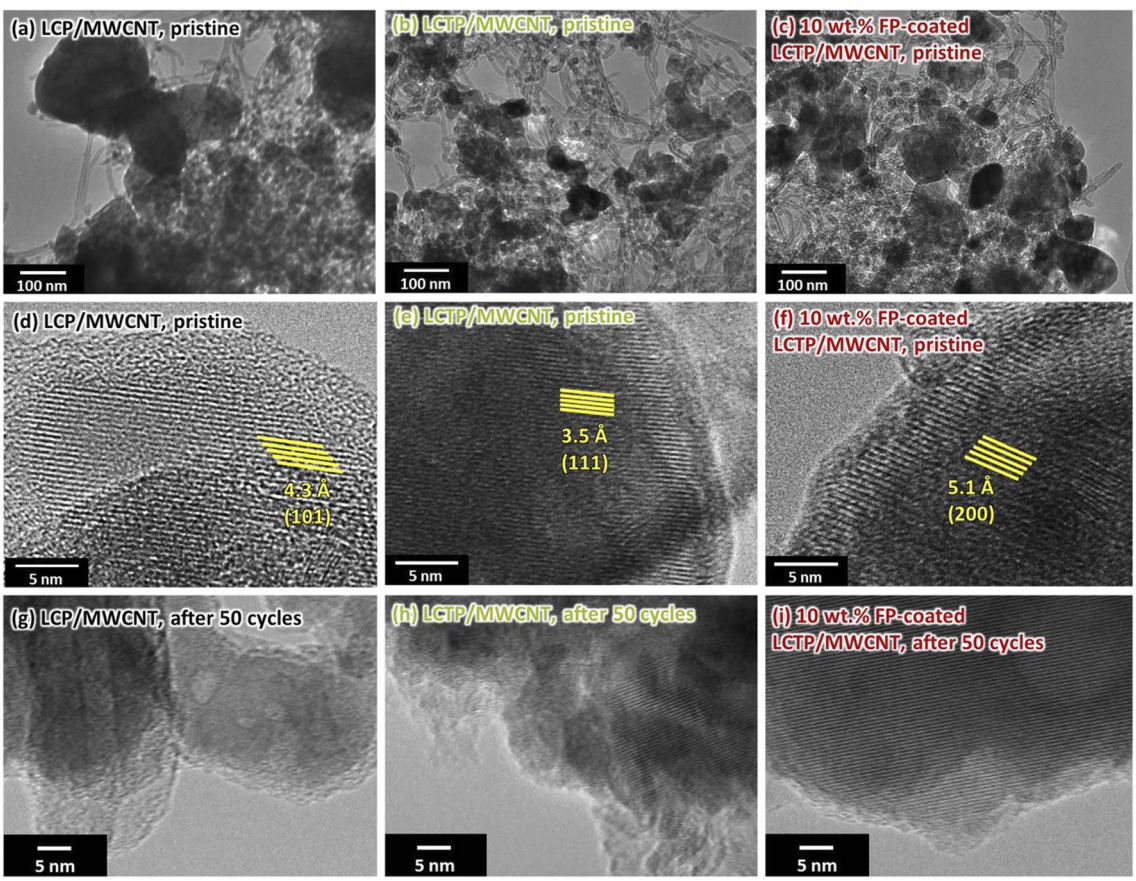

Fig. 4 Lower-magnification (10 000×) higher-resolution TEM images (a–c) and magnified (400 000×) HRTEM images (d–i) for different samples; pristine LCP/MWCNT (a), (d), pristine LCTP/MWCNT (b), (e), pristine FP-coated LCTP/MWCNT (c), (f), after 50 cycles LCP/MWCNT (g), after 50 cycles LCTP/MWCNT (h), and after 50 cycles FP-coated LCTP/MWCNT (i).

term cyclability, while Ti^{4+}-substitution contributes to the higher utilization of Co in LCTP crystals.

Conclusion

In conclusion, 10 wt% FP-coated LCTP sample showed a higher discharge capacity of 116 mA h g^{-1} together with stable cycle performance over 99% of capacity retention at 100th cycle. The Fe^{3+}-rich surface on LCP samples is formed during FP-coating and prevents from irreversible crystal structure change and electrolyte decomposition during cycling, resulting in stable cycle performance. Further doping LCP with Ti^{4+} allows, by charge compensation mechanism, for the creation of vacancies in Co sites together with an unexpected stabilization of Co in 2+ valence state in the pristine material, which results in improvement of the capacity. The combination of FP-coating and Ti^{4+}-substitution, leads to improved cycling stability with higher capacity compared with LCP. Our findings offer new strategies for improving cycle performance without sacrificing the capacity of LCP, paving the way toward the realization of high voltage Li-ion batteries.

Experimental

Materials

$Co(CH_3COO)_2 \cdot 4H_2O$ (>99%, Wako Pure Chemicals), $Fe(CH_3COO)_2$ (>99%, Sigma-Aldrich Corp.), CH_3COOLi (>98.0%, Wako Pure Chemicals), $Ti_2(SO_4)_3$ aq. (45% in H_2SO_4, Sigma-Aldrich), and H_3PO_4 (>85.0%, Wako Pure Chemicals) were used to prepare $LiCoPO_4$ (LCP), $LiCo_{1-2x}Ti_xPO_4$ (LCTP), and $FePO_4$-coated compounds. Citric acid ($C_6H_8O_7$) (>99.5%, Sigma-Aldrich Corp.) was used as a chelating agent. Multiwalled carbon nanotubes (MWCNTs) with a specific surface area of 240 m^2 g^{-1} were used for the preparation of carbon composite. Distilled water (17 MΩ cm) was used a medium for the entire preparation scheme.

Preparation of LCP/MWCNT and LCTP/MWCNT composites under UC treatment

LCP/MWCNT composite was synthesized *via* UC treatment as previously reported.[20] Similar scheme of LCP was applied to synthesize LCTP/MWCNT composite. First, two kinds of solutions (solution A and B) were prepared. The solution A was composed of 0.4000 g of MWCNT and 0.6714 g of H_3PO_4 (1.0 eq. for LCTP) mixed in 50 ml of ultrapure water. The solution B was composed of 1.3432 g of $Co(CH_3COO)_2 \cdot 4H_2O$ (0.9 eq.), 0.1265 g of $Ti_2(SO_4)_3$ (0.05 eq.), 0.3994 g of CH_3COOLi (1.0 eq.) and 1.1454 g of citric acid (1.0 eq.) dissolved in 20 ml of ultrapure water. The solution A was subjected to the UC treatment at 80 °C for 5 min before and after the addition of the solution B. The UC-treated sol was further dried at 130 °C under vacuum for 12 h. The obtained powder made of LCTP precursor and MWCNT was pre-annealed at 350 °C in air for 1 h to remove absorbed water and citric-acid-derived amorphous carbon, then left to cool down to room temperature (RT). The pre-annealed powder was then fast annealed at 650 °C under N_2 flow (RT to 650 °C in 3 min, dwell for 30 min, 20 min to cooling to RT) to form the LCTP/MWCNT composite. The pristine LCTP/MWCNT composite was further annealed at 350 °C for 3 h under air in order to oxidize Ti^{3+} into Ti^{4+} and to obtain vacancy in LCTP crystals without decomposing MWCNTs.

Preparation of $FePO_4$-coated LCTP/MWCNT composite

In case of FP-coating, another two kinds of solutions (solution C and D) were prepared. The solution C was composed of 0.2500 g of synthesized LCTP/MWCNT and 0.0183 g of H_3PO_4 (1.0 eq. for FP) mixed in 10 ml of ultrapure water. The solution D was composed of 0.0276 g of $Fe(CH_3COO)_2$ (0.05 eq.), 0.0107 g of CH_3COOLi (1.0 eq.) and 0.0306 g of citric acid (1.0 eq.) dissolved in 10 ml of ultrapure water. Mixture of solution C and D were then subjected to UC treatment at 80 °C for 5 min. The UC-treated sol was further dried at 130 °C under vacuum for 12 h. Then, same annealing process was applied to dried powder to obtain FP-coated samples. The obtained powder was pre-annealed at 350 °C in air for 1 h, then left to cool down to RT. The pre-annealed powder was then fast annealed at 700 °C under N_2 flow (RT to 700 °C in 3 min, dwell for 5 min, 20 min to cooling to RT). The pristine LFP-coated composite was further annealed at 350 °C for 3 h under air in order to form FP-coated samples.

Physicochemical characterizations of LCP/MWCNT, LCTP/MWCNT, and $FePO_4$-coated LCTP/MWCNT composites

Structure analysis on LCP/MWCNT, LCTP/MWCNT, and FP-coated LCTP/MWCNT composites were performed by X-ray diffraction [XRD, Smart-lab (Rigaku)] using Cu Kα radiation (λ = 1.54 Å). XRD patterns were recorded in the 10–90° 2θ range at a scan speed of 0.0033° s^{-1}. Time-of-flight neutron powder diffraction (NPD) measurements were performed at the iMATERIA (BL20) facility of the Japan Photon Accelerator Research Complex (J-PARC, Ibaraki, Japan) to obtain NPD patterns corresponding to 0.5–4.8 Å in *d*-spacing. The carbon contents of composites were determined by thermogravimetric analysis under a synthetic air (O_2: 20%, N_2: 80%) using a thermogravimetric/differential thermal analyzer (TG/DTA, Seiko Instruments TG/DTA6300). X-ray photoelectron spectroscopy [XPS, JPS-9200 (JEOL)] was carried out using Mg X-ray source. X-ray adsorption fine structure (XAFS) measurements at the Co, Fe, and Ti K-edges for composites were performed in transmission mode at the beam line BL01 of the synchrotron radiation facility SPring-8 (Hyogo, Japan). Laminate-type two-electrode cells were assembled using lithium metal foil as a negative electrode and composites as a positive electrode. The obtained XAFS spectra were analyzed using the spectral fitting software REX2000 (Rigaku Corp.) to evaluate the ratio of Co and Fe species with references at different oxidation states, such as Co^{2+} ($LiCoPO_4$ bulk sample), Co^{3+} (Cobalt acetylacetonate), Fe^{2+} ($LiFePO_4$ bulk sample), Fe^{3+} ($FePO_4$ bulk sample oxidized by the chemical method using NO_2BF_4), Ti^{3+} (Ti_2O_3), and Ti^{4+} (TiO_2 rutile).

Electrochemical characterization of LCP/MWCNT, LCTP/MWCNT, and $FePO_4$-coated LCTP/MWCNT composites

Half-cells were assembled using a negative Li metal electrode, a positive LCP/MWCNT, LCTP/MWCNT, and FP-coated LCTP/MWCNT electrode in 2032 coin-type cells. The electrolyte was a mixture of ethylene carbonate, propyl carbonate and dimethyl carbonate (EC : PC : DMC = 1 : 1 : 3) containing 1.0 M $LiPF_6$. Positive electrode was prepared by mixing 90 wt% of the composite and 10 wt% of polyvinylidene difluoride in *N*-methyl pyrrolidone. The mixture was coated on an etched-Al foil (current collector) and dried at 80 °C in vacuum for 12 h. The mass loading of the composite was 1.4 mg cm^{-2} on etched Al current collector (1.54 cm^2). Charge/discharge tests were performed at constant-current constant-voltage mode between 4.3 and 5.0 V *vs.* Li^+/Li at current density of 0.2C-rate, assuming that 1C-rate equals 167 mA g^{-1}. The cut-off current density at the constant-voltage (CC–CV) mode was 8.35 mA g^{-1} (0.05C). Before charge–discharge tests, a pre-cycling was conducted at 0.1C in the same potential range as charge–discharge tests.

Conflicts of interest

There are no conflicts to declare.

Acknowledgements

This study was supported by JSPS Grant-in-Aid for Scientific Research (KAKENHI) A under Grant No. JP19H00882 and KAKENHI Grant-in-Aid for Early-Career Scientists under Grant No. JP21K14711.

References

1 K. Amine, H. Yasuda and M. Yamachi, Olivine $LiCoPO_4$ as 4.8 V Electrode Material for Lithium Batteries, *Electrochem. Solid-State Lett.*, 2000, **3**(4), 178–179, DOI: 10.1149/1.1390994.

2 Y.-M. Kang, Y.-I. Kim, M.-W. Oh, R.-Z. Yin, Y. Lee, D.-W. Han, H.-S. Kwon, J. H. Kim and G. Ramanath, Structurally stabilized olivine lithium phosphate cathodes with enhanced electrochemical properties through Fe doping, *Energy Environ. Sci.*, 2011, **4**(12), 4978, DOI: 10.1039/c1ee02283k.

3 M. Zhang, N. Garcia-Araez and A. L. Hector, Understanding and development of olivine $LiCoPO_4$ cathode materials for lithium-ion batteries, *J. Mater. Chem. A*, 2018, **6**(30), 14483–14517, DOI: 10.1039/C8TA04063J.

4 A. Mauger, C. M. Julien, M. Armand, J. B. Goodenough and K. Zaghib, Li(Ni,Co)PO_4 as cathode materials for lithium batteries: Will the dream come true?, *Curr. Opin. Electrochem.*, 2017, **6**(1), 63–69, DOI: 10.1016/j.coelec.2017.10.015.

5 A. Blyr, C. Sigala, G. Amatucci, D. Guyomard, Y. Chabre and J. M. Tarascon, Self-Discharge of $LiMn_2O_4$/C Li-Ion Cells in Their Discharged State: Understanding by Means of Three-Electrode Measurements, *J. Electrochem. Soc.*, 1998, **145**(1), 194–209, DOI: 10.1149/1.1838235.

6 Q. Zhong, A. Bonakdarpour, M. Zhang, Y. Gao and J. R. Dahn, Synthesis and Electrochemistry of $LiNi_xMn_2 - xO_4$, *J. Electrochem. Soc.*, 1997, **144**(1), 205–213, DOI: 10.1149/1.1837386.

7 S. J. Wen, T. J. Richardson, L. Ma, K. A. Striebel, P. N. Boss and E. J. Cairns, FTIR Spectroscopy of Metal Oxide Insertion Electrodes: A New Diagnostic Tool for Analysis of Capacity Fading in Secondary Cells, *J. Electrochem. Soc.*, 1996, **143**(6), L136–L138, DOI: 10.1149/1.1836902.

8 F. Zhou, M. Cococcioni, C. A. Marianetti, D. Morgan and G. Ceder, First-principles prediction of redox potentials in transition-metal compounds with LDA + U, *Phys. Rev. B*, 2004, **70**(23), 235121, DOI: 10.1103/PhysRevB.70.235121.

9 L. Liu, H. Zhang, X. Chen, L. Fang, Y. Bai, R. Liu and Y. Wang, Unique synthesis of sandwiched graphene@($Li_{0.893}Fe_{0.036}$)$Co(PO_4)$ nanoparticles as high-performance cathode materials for lithium-ion batteries, *J. Mater. Chem. A*, 2015, **3**(23), 12320–12327, DOI: 10.1039/c5ta02058a.

10 J. Xie, N. Imanishi, T. Zhang, A. Hirano, Y. Takeda and O. Yamamoto, Li-ion diffusion kinetics in $LiCoPO_4$ thin films deposited on NASICON-type glass ceramic electrolytes by magnetron sputtering, *J. Power Sources*, 2009, **192**(2), 689–692, DOI: 10.1016/j.jpowsour.2009.03.001.

11 E. Markevich, G. Salitra, K. Fridman, R. Sharabi, G. Gershinsky, A. Garsuch, G. Semrau, M. A. Schmidt and D. Aurbach, Fluoroethylene Carbonate as an Important Component in Electrolyte Solutions for High-Voltage Lithium Batteries: Role of Surface Chemistry on the Cathode, *Langmuir*, 2014, **30**(25), 7414–7424, DOI: 10.1021/la501368y.

12 E. Markevich, R. Sharabi, H. Gottlieb, V. Borgel, K. Fridman, G. Salitra, D. Aurbach, G. Semrau, M. A. Schmidt, N. Schall, *et al.*, Reasons for capacity fading of $LiCoPO_4$ cathodes in $LiPF_6$ containing electrolyte solutions, *Electrochem. Commun.*, 2012, **15**(1), 22–25, DOI: 10.1016/j.elecom.2011.11.014.

13 N. N. Bramnik, K. Nikolowski, D. M. Trots and H. Ehrenberg, Thermal Stability of $LiCoPO_4$ Cathodes, *Electrochem. Solid-State Lett.*, 2008, **11**(6), A89–A93, DOI: 10.1149/1.2894902.

14 H. Ehrenberg, N. N. Bramnik, A. Senyshyn and H. Fuess, Crystal and magnetic structures of electrochemically delithiated $Li_{1-x}CoPO_4$ phases, *Solid State Sci.*, 2009, **11**(1), 18–23, DOI: 10.1016/j.solidstatesciences.2008.04.017.

15 R. Sharabi, E. Markevich, K. Fridman, G. Gershinsky, G. Salitra, D. Aurbach, G. Semrau, M. A. Schmidt, N. Schall and C. Bruenig, Electrolyte solution for the improved cycling performance of $LiCoPO_4$/C composite cathodes, *Electrochem. Commun.*, 2013, **28**, 20–23, DOI: 10.1016/j.elecom.2012.12.001.

16 J. L. Allen, T. Thompson, J. Sakamoto, C. R. Becker, T. R. Jow and J. Wolfenstine, Transport properties of $LiCoPO_4$ and Fe-substituted $LiCoPO_4$, *J. Power Sources*, 2014, **254**, 204–208, DOI: 10.1016/j.jpowsour.2013.12.111.

17 J. L. Allen, J. L. Allen, T. Thompson, S. A. Delp, J. Wolfenstine and T. R. Jow, Cr and Si Substituted-$LiCo_{0.9}Fe_{0.1}PO_4$: Structure, full and half Li-ion cell performance, *J. Power Sources*, 2016, **327**, 229–234, DOI: 10.1016/j.jpowsour.2016.07.055.

18 J. L. Allen, T. R. Jow and J. Wolfenstine, Improved cycle life of Fe-substituted $LiCoPO_4$, *J. Power Sources*, 2011, **196**(20), 8656–8661, DOI: 10.1016/j.jpowsour.2011.06.057.

19 R. Hanafusa, Y. Oka and T. Nakamura, Electrochemical and Magnetic Studies of Li-Deficient $Li_{1-x}Co_{1-x}Fe_xPO_4$ Olivine Cathode Compounds, *J. Electrochem. Soc.*, 2015, **162**(2), A3045–A3051, DOI: 10.1149/2.0071502jes.

20 N. Okita, K. Kisu, E. Iwama, Y. Sakai, Y. Lim, Y. Takami, M. T. Sougrati, T. Brousse, P. Rozier, P. Simon, W. Naoi and K. Naoi, Stabilizing the Structure of $LiCoPO_4$ Nanocrystals *via* Addition of Fe^{3+}: Formation of Fe^{3+} Surface Layer, Creation of Diffusion-Enhancing Vacancies, and Enabling High-Voltage Battery Operation, *Chem. Mater.*, 2018, **30**(19), 6675–6683, DOI: 10.1021/acs.chemmater.8b01965.

21 N. Okita, E. Iwama, Y. Takami, S. Abo, W. Naoi, M. T. H. Reid and K. Naoi, Crystal-structure-matched $FePO_4$ Surface-coating on $LiCoPO_4$/MWCNT Nanocomposites for Long Lifecycle 5 V Class Lithium Ion Batteries, *Electrochemistry*, 2019, **87**(3), 156–161, DOI: 10.5796/electrochemistry.18-00096.

22 K. J. Kreder and A. Manthiram, Vanadium-Substituted $LiCoPO_4$ Core with a Monolithic $LiFePO_4$ Shell for High-Voltage Lithium-Ion Batteries, *ACS Energy Lett.*, 2017, **2**(1), 64–69, DOI: 10.1021/acsenergylett.6b00496.

23 I. C. Jang, C. G. Son, S. M. G. Yang, J. W. Lee, A. R. Cho, V. Aravindan, G. J. Park, K. S. Kang, W. S. Kim, W. I. Cho and Y. S. Lee, $LiFePO_4$ modified $Li_{1.02}(Co_{0.9}Fe_{0.1})_{0.98}PO_4$ cathodes with improved lithium storage properties, *J. Mater. Chem.*, 2011, **21**(18), 6510–6514, DOI: 10.1039/C1JM10574D.

24 A. M. Aboraia, M. G. Moustafa, V. V. Shapovalov, A. A. Guda, F. Elmasry and A. Soldatov, Enhancement of the electrochemical performance of $LiCoPO_4$ by Fe doping, *Ceram. Int.*, 2021, **47**(22), 31826–31833, DOI: 10.1016/j.ceramint.2021.08.065.

25 S. Brutti, J. Manzi, D. Meggiolaro, F. M. Vitucci, F. Trequattrini, A. Paolone and O. Palumbo, Interplay between local structure and transport properties in iron-doped $LiCoPO_4$ olivines, *J. Mater. Chem. A*, 2017, **5**(27), 14020–14030, DOI: 10.1039/c7ta03161k.

26 F. Wang, J. Yang, Y. NuLi and J. Wang, Highly promoted electrochemical performance of 5 V $LiCoPO_4$ cathode material by addition of vanadium, *J. Power Sources*, 2010, **195**(19), 6884–6887, DOI: 10.1016/j.jpowsour.2010.04.071.

27 W. Zhu, D. Liu, C. Gagnon, V. Gariepy, M. L. Trudeau, A. Vijh and K. Zaghib, Phase Transformation of Doped $LiCoPO_4$ during Galvanostatic Cycling, *Materials*, 2020, **13**(17), 3810, DOI: 10.3390/ma13173810.

28 D. Zhang, Rapid synthesis of $LiCo_{1-x}Fe_xPO_4$/C Cathodes *via* Microwave Solvothermal Method for Li-ion Batteries, *Int. J. Electrochem. Sci.*, 2018, 2544–2555, DOI: 10.20964/2018.03.61.

29 H. Li, Y. Wang, X. Yang, L. Liu, L. Chen and J. Wei, Improved electrochemical performance of 5 V $LiCoPO_4$ cathode materials *via* yttrium doping, *Solid State Ionics*, 2014, **255**, 84–88, DOI: 10.1016/j.ssi.2013.12.007.